Journal of Sound and Vibration 331 (2012) 5268–5282

Contents lists available at SciVerse ScienceDirect

Journal of Sound and Vibration

journal homepage: www.elsevier.com/locate/jsvi

Dynamic response of thin-walled structures by variable kinematic one-dimensional models

E. Carrera, A. Varello*

Department of Mechanical and Aerospace Engineering, Politecnico di Torino, Corso Duca degli Abruzzi 24, 10129 Torino, Italy

ARTICLE INFO

Article history:
Received 30 January 2012
Received in revised form
1 June 2012
Accepted 2 July 2012
Handling Editor: S. Ilanko
Available online 3 August 2012

ABSTRACT

This paper investigates the accuracy capabilities of using variable kinematic modeling in compact and thin-walled beam-like structures with dynamic loadings. Carrera Unified Formulation (CUF) is employed to introduce refined one-dimensional (1D) models with a variable order of expansion for the displacement unknowns over the beam cross-section. Classical Euler–Bernoulli and Timoshenko beam theories are obtained as particular cases of these variable kinematic models while a higher order expansion permits the detection of in-plane cross-section deformation, since it leads to shell-like solutions. Finite element (FE) method is used to provide numerical results and the Newmark method is implemented as a time integration scheme. Some assessments with closed form solutions are discussed and comparisons with shell-type results obtained with commercial FE software are made. Further analyses address both compact and thin-walled cross-sections. In particular, the case of a deformable thin-walled cylinder loaded by time-dependent internal forces is discussed. The results clearly show that finite elements which are formulated in the CUF framework do not introduce additional numerical problems with respect to classical beam theories. Comparisons with elasticity solutions prove that the present 1D CUF model offers an accuracy in analyzing thin-walled structures which is typical of shell or three-dimensional models with a remarkable reduction in the computational cost required.

1. Introduction

Nowadays different kinds of slender structures are involved in many areas such as aerospace, civil and biomechanical engineering. There are many examples of these one-dimensional (1D) structures such as rotor and wind blades, aircraft wings, bridges and towers, and even arteries. Such beam-like components can be analyzed by means of 1D formulations and one main advantage is that 1D models require a lower computational cost compared with 2D plate and shell or 3D solid models [1].

The 1D models used in early studies of slender structures were based on classical theories. Euler–Bernoulli theory [2] neglected the transverse shear deformation completely. The first shear deformation theory of Timoshenko [3] assumed a constant shear strain across the cross-section. The growing use of advanced composite and sandwich materials in thin-walled beam-like structures has revealed that 1D theories have to be refined in order to predict the behavior of such

* Corresponding author. Tel.: +39 011 090 6871; fax: +39 011 090 6899.
E-mail addresses: erasmo.carrera@polito.it (E. Carrera), alberto.varello@polito.it (A. Varello).
URL: http://www.mul2.com (A. Varello).

0022-460X/$ - see front matter © 2012 Elsevier Ltd. All rights reserved.
http://dx.doi.org/10.1016/j.jsv.2012.07.006

complex structures in an accurate way. Moreover, refined 1D theories are necessary to cope with arbitrary cross-section geometries, short beams, nonhomogeneous sections and curved shapes by taking into account effects such as warping and in-plane cross-section deformation. In the past, many theoretical and computational approaches were taken to address these issues. Recently, refined theories such as those based on the 1D Carrera Unified Formulation (CUF) [4,5] and variational asymptotic methods (VABS) [6] as well as the Generalized Beam Theory (GBT) [7] have presented remarkable advances in static, buckling, and free vibration analysis.

Most beam-like structural systems in physical applications are actually subjected to dynamic loadings of all kinds, for instance, blood flow in arteries [8]; lifting systems under the action of unsteady aerodynamic pressures [9]; blast and sonic-boom loadings [10]; interaction between bridges and moving vehicles [11]; impulsive loadings by missile launch or impact on aircraft wings [12]; and the effect of seismic waves on buildings [13]. Hence, an accurate understanding of the dynamic characteristics of a large number of structures is crucial in engineering. The importance of refined 1D models is even more relevant for accurate prediction of the time-dependent response of thin-walled slender structures [14].

A detailed review of several theories for vibrations and wave propagation was presented by Kapania and Raciti [15]. A brief, though not exhaustive, review of refined 1D models introduced in recent decades for the dynamic analysis of beams is presented here. A second-order theory with cross-sectional warping was proposed by Stephen and Levinson [16]. Heyliger and Reddy [17] and Soldatos and Elishakoff [18] proposed a third-order theory with a quadratic variation of the shear strain across the cross-section. Early fourth-order beam theories were formulated by Levinson [19], Rychter [20] and were extended by Bickford [21] to the dynamic analysis. Kant and Gupta [22] proposed a refined FE higher order model with quadratic transverse shear strain that was applied to the free vibration analysis of angle-ply laminated, deep sandwich and composite beams [23,24]. Kant et al. [25] provided an analytical solution to the natural frequency analysis of thick and thin composite beams by accurately describing the cross-section warping. The formulation of two higher order shear deformation theories by Subramanian [26] satisfied the traction-free surface conditions at the top and bottom beam surfaces. A higher order FE model based on classical laminated theory presented higher frequencies analysis capabilities for the vibration response of laminated tapered beams [27,28]. Recently, Şimşek and Kocatürk [29] highlighted that a third-order shear deformation theory gives significantly better results than classical theories in the case of short beams and high mode numbers.

As far as the dynamic response is concerned, many shear deformable models have been introduced in last decades. Tong et al. [30] offered an analytical solution for free and forced vibrations of stepped generally nonuniform Timoshenko beams. A higher order shear deformation theory was used by Rao and Ganesan [31] to evaluate the harmonic response of tapered composite wings. Marur and Kant extended their work [23] to the transient dynamic analysis of symmetric and unsymmetric sandwich and composite structures [14]. The efficacy of higher order terms in predicting displacements and stress resultants in time was clearly brought out. By involving the action of a moving dynamic load, the importance of third-order shear deformation effect in the strength analysis of cross-ply and angle-ply laminated beams was highlighted even when the slender ratio is not very low [32]. Librescu and Na [33] used a nonclassical beam model which includes transverse shear, secondary warping and heterogeneity to control the bending oscillations of cantilevers subjected to time-dependent excitations. The same authors [34] studied nonuniform anisotropic thin-walled beams incorporating adaptive capabilities through a beam model with transverse shear and warping inhibition which was formulated in [10]. Piovan and Cortínez [35] developed a new theoretical model for the generalized linear analysis of composite thin-walled curved beams with open and closed arbitrary cross-sections, by showing the influence of shear deformability on the mechanics of such complex structures. As a particular case of dynamic response, the third-order shear deformation theory used by Şimşek [36] indicated the importance of higher order terms in correctly predicting the dynamic behavior of functionally graded beams and thus in tailoring FG material properties.

As mentioned, higher order 1D models with generalized displacement variables based on CUF have recently been proposed by Carrera and co-authors for the analysis of isotropic [5,37] and composite structures [38,39]. CUF has been developed over the last decade for plate/shell models [40] and it has recently been extended to static and dynamic 1D modeling [4,41,42]. CUF is a hierarchical formulation which considers the order of the model as a free-parameter of the analysis. In other words, models of any order can be obtained with no need for *ad hoc* formulations by exploiting a systematic procedure.

The first extension of 1D CUF finite elements to the free vibration analysis of beams with arbitrary section geometries was done in [43]. These models were afterwards employed to carry out a more accurate free vibration analysis of conventional and joined wings [42]. Higher order terms permitted bending/torsion modes to be coupled and were able to capture any other vibration modes that require in-plane and warping deformation of the beam sections to be detected.

In this paper, the extension of one-dimensional CUF models to the dynamic response analysis of slender structures is presented. Taylor-like polynomial expansions are adopted for the displacement field. The finite element method is used to handle arbitrary geometries and loading conditions. The Newmark time integration method [1], widely used in structural dynamics, is employed. A preliminary assessment to test the accuracy of the present FEs is carried out on reference cases retrieved from the structural dynamics literature. A number of thin-walled configurations (obtained by varying span-to-height ratio, cross-section geometry and boundary conditions) subjected to time-dependent loadings such as harmonic and traveling ones are afterwards analyzed. The influence of higher order effects over the cross-section deformation, not detectable by classical and low-order beam theories, on the time-dependent response of the structures considered is enhanced. The use of variable kinematic 1D CUF models in the Newmark time integration scheme reveals their shell-type capabilities in accurately describing the dynamic behavior of thin-walled structures.

2. Preliminaries

A slender structure with axial length L is considered and studied as a beam. The intersection of the beam with a plane that is perpendicular to its axis identifies the beam's cross-section Ω. A local cartesian coordinate system composed of x- and z-axes parallel to the cross-section plane is defined, whereas y represents the out-of-plane coordinate. However, the y-axis is not necessarily a centroidal one. For instance, in the case of an arbitrarily oriented beam, the local y-axis might not be the beam geometrical axis. This gives high versatility to the present structural beam model. The cartesian components of the displacement vector $\mathbf{u}(x,y,z,t)$ are u_x, u_y, and u_z. The stress $\boldsymbol{\sigma}$ and the strain $\boldsymbol{\varepsilon}$ are grouped in vectors as follows:

$$\begin{aligned} \boldsymbol{\sigma}_p &= \{\sigma_{zz}\ \sigma_{xx}\ \sigma_{zx}\}^T, \quad \boldsymbol{\varepsilon}_p = \{\varepsilon_{zz}\ \varepsilon_{xx}\ \varepsilon_{zx}\}^T \\ \boldsymbol{\sigma}_n &= \{\sigma_{zy}\ \sigma_{xy}\ \sigma_{yy}\}^T, \quad \boldsymbol{\varepsilon}_n = \{\varepsilon_{zy}\ \varepsilon_{xy}\ \varepsilon_{yy}\}^T \end{aligned} \tag{1}$$

where superscript T stands for the transposition operator. Subscript p refers to quantities related to the beam cross-section Ω, whereas subscript n refers to quantities related to the out-of-plane direction. In the case of small displacements with respect to the length L, the linear relations between strain and displacement components hold and a compact vectorial notation can be adopted:

$$\begin{aligned} \boldsymbol{\varepsilon}_p &= \mathbf{D}_p \mathbf{u} \\ \boldsymbol{\varepsilon}_n &= \mathbf{D}_n \mathbf{u} = \mathbf{D}_{np}\mathbf{u} + \mathbf{D}_{ny}\mathbf{u} \end{aligned} \tag{2}$$

where $\mathbf{D}_p$, $\mathbf{D}_{np}$, and $\mathbf{D}_{ny}$ are differential matrix operators:

$$\mathbf{D}_p = \begin{bmatrix} 0 & 0 & \frac{\partial}{\partial z} \\ \frac{\partial}{\partial x} & 0 & 0 \\ \frac{\partial}{\partial z} & 0 & \frac{\partial}{\partial x} \end{bmatrix}, \quad \mathbf{D}_{np} = \begin{bmatrix} 0 & \frac{\partial}{\partial z} & 0 \\ 0 & \frac{\partial}{\partial x} & 0 \\ 0 & 0 & 0 \end{bmatrix}, \quad \mathbf{D}_{ny} = \begin{bmatrix} 0 & 0 & \frac{\partial}{\partial y} \\ \frac{\partial}{\partial y} & 0 & 0 \\ 0 & \frac{\partial}{\partial y} & 0 \end{bmatrix} \tag{3}$$

According to Eq. (1), the generalized Hooke's law for isotropic materials is

$$\begin{aligned} \boldsymbol{\sigma}_p &= \mathbf{C}_{pp}\boldsymbol{\varepsilon}_p + \mathbf{C}_{pn}\boldsymbol{\varepsilon}_n \\ \boldsymbol{\sigma}_n &= \mathbf{C}_{np}\boldsymbol{\varepsilon}_p + \mathbf{C}_{nn}\boldsymbol{\varepsilon}_n \end{aligned} \tag{4}$$

where matrices $\mathbf{C}_{pp}$, $\mathbf{C}_{pn}$, $\mathbf{C}_{np}$ and $\mathbf{C}_{nn}$ are

$$\mathbf{C}_{pp} = \begin{bmatrix} C_{11} & C_{12} & 0 \\ C_{12} & C_{22} & 0 \\ 0 & 0 & C_{44} \end{bmatrix}, \quad \mathbf{C}_{pn} = \mathbf{C}_{np}^T = \begin{bmatrix} 0 & 0 & C_{13} \\ 0 & 0 & C_{23} \\ 0 & 0 & 0 \end{bmatrix},$$
$$\mathbf{C}_{nn} = \begin{bmatrix} C_{55} & 0 & 0 \\ 0 & C_{66} & 0 \\ 0 & 0 & C_{33} \end{bmatrix} \tag{5}$$

For the sake of brevity, the dependence of the coefficients C_{ij} on Young's modulus, Poisson's ratio, and shear modulus is not reported here. It can be found in Jones [44]. In this paper isotropic materials are considered. The extension to composite beams will be presented in future papers.

3. Variable kinematic 1D models

According to the framework of Carrera Unified Formulation (CUF) [5], the displacement field is assumed to be an expansion of a certain class of functions F_τ, which depend on the cross-section coordinates x and z:

$$\mathbf{u}(x,y,z,t) = F_\tau(x,z)\mathbf{u}_\tau(y,t), \quad \tau = 1,2,\ldots,N_u = N_u(N) \tag{6}$$

The compact expression is based on Einstein's notation: repeated subscript τ indicates summation. The number of expansion terms N_u depends on the expansion order N, which is a free parameter of the formulation. Taylor's polynomials are chosen as cross-section functions F_τ. Most displacement-based theories can be formulated on the basis of the above generic kinematic field. For instance, when $N=2$, the second-order axiomatic displacement field is given by

$$\begin{aligned} u_x &= u_{x1} + u_{x2}x + u_{x3}z + u_{x4}x^2 + u_{x5}xz + u_{x6}z^2 \\ u_y &= u_{y1} + u_{y2}x + u_{y3}z + u_{y4}x^2 + u_{y5}xz + u_{y6}z^2 \\ u_z &= u_{z1} + u_{z2}x + u_{z3}z + u_{z4}x^2 + u_{z5}xz + u_{z6}z^2 \end{aligned} \tag{7}$$

Subsequently, the classical beam models such as Euler–Bernoulli's (EBBM) [2] and Timoshenko's (TBM) [3] are easily derived from the first-order approximation model. Timoshenko beam model (TBM) can be obtained by setting terms $\{u_{ij} : i = x,z; j = 2,3\}$ equal to zero. In addition, an infinite rigidity in the transverse shear is also adopted for EBBM by

penalizating ε_{yz} and ε_{xy} via a high penalty value in the following constitutive equations:

$$\sigma_{yz} = C_{55}\varepsilon_{yz}, \quad \sigma_{xy} = C_{66}\varepsilon_{xy} \tag{8}$$

Higher order models provide an accurate description of the shear mechanics, the cross-section deformation, Poisson's effect along the spatial directions and the torsional mechanics in more detail than classical models do. EBBM neglects them all, since it was formulated to describe the bending mechanics. TBM takes into account constant shear stress and strain components. Classical theories and first-order models require the assumption of opportunely reduced material stiffness coefficients to correct Poisson's locking effect [45,46]. According to Carrera and Giunta [4], the same technique is used here to correct Poisson's locking.

4. Finite element formulation

Following standard FEM, the unknown variables in the element domain are expressed in terms of their values corresponding to the element nodes [5]. For the sake of completeness, some details about the formulation of CUF finite elements are here retrieved from previous works [42,43] and extended to the dynamic response analysis. By introducing the shape functions N_i and the nodal displacement vector $\mathbf{q}$, the displacement field becomes:

$$\mathbf{u}(x,y,z,t) = F_\tau(x,z)N_i(y)\mathbf{q}_{\tau i}(t), \quad i = 1,2,\ldots,N_N \tag{9}$$

where

$$\mathbf{q}_{\tau i} = \{q_{u_{x\tau i}}\ q_{u_{y_{\tau i}}}\ q_{u_{z\tau i}}\}^T \tag{10}$$

contains the degrees of freedom of the τ^{th} expansion term corresponding to the i^{th} element node. Elements with N_N number of nodes equal to 2, 3 and 4 are formulated and named $B2$, $B3$, and $B4$, respectively. The results reported in the present work involve only $B4$ elements. For the sake of brevity, more details are not reported here, but can be found in Carrera et al. [41,43]. This beam model can be easily extended to mixed theories. However, this work presents a displacement-based formulation. The variational statement is therefore the Principle of Virtual Displacements:

$$\delta L_{\text{int}} = \int_V (\delta\boldsymbol{\varepsilon}_n^T\boldsymbol{\sigma}_n + \delta\boldsymbol{\varepsilon}_p^T\boldsymbol{\sigma}_p)\,\mathrm{d}V = \delta L_{\text{ext}} - \delta L_{\text{ine}} \tag{11}$$

where L_{int} is the internal strain energy, L_{ext} is the work of external loadings, and L_{ine} is the work of inertial loadings. δ stands for the virtual variation. The damping effect is neglected for the sake of simplicity. Substituting Eq. (9) into Eq. (2) and using the fact that F_τ are independent of y, the strain vectors can be written as

$$\boldsymbol{\varepsilon}_n = (\mathbf{D}_{np}F_\tau\mathbf{I})N_i\mathbf{q}_{\tau i} + F_\tau(\mathbf{D}_{ny}N_i\mathbf{I})\mathbf{q}_{\tau i}, \quad \boldsymbol{\varepsilon}_p = (\mathbf{D}_pF_\tau\mathbf{I})N_i\mathbf{q}_{\tau i} \tag{12}$$

where $\mathbf{I}$ is the identity matrix. The expression of the internal strain energy (Eq. (11)) can be rewritten in terms of virtual nodal displacements as follows:

$$\delta L_{\text{int}} = \delta\mathbf{q}_{\tau i}^T\ \mathbf{K}^{ij\tau s}\ \mathbf{q}_{sj} \tag{13}$$

where Eq. (4) has been used. The 3×3 *fundamental nucleus* of the structural stiffness matrix presented in Eq. (13) can be shown to have the following explicit equation:

$$\begin{aligned}\mathbf{K}^{ij\tau s} = {} & E_{ij} \lhd (\mathbf{D}_{np}^T F_\tau\mathbf{I})[\mathbf{C}_{np}(\mathbf{D}_pF_s\mathbf{I}) + \mathbf{C}_{nn}(\mathbf{D}_{np}F_s\mathbf{I})] + (\mathbf{D}_p^T F_\tau\mathbf{I})[\mathbf{C}_{pp}(\mathbf{D}_pF_s\mathbf{I}) + \mathbf{C}_{pn}(\mathbf{D}_{np}F_s\mathbf{I})] \rhd_\Omega \\ & + E_{ij,_y} \lhd [(\mathbf{D}_{np}^T F_\tau\mathbf{I})\mathbf{C}_{nn} + (\mathbf{D}_p^T F_\tau\mathbf{I})\mathbf{C}_{pn}]F_s \rhd_\Omega \mathbf{I}_{\Omega y} + E_{i,yj}\mathbf{I}_{\Omega y}^T \lhd F_\tau[\mathbf{C}_{np}(\mathbf{D}_pF_s\mathbf{I}) + \mathbf{C}_{nn}(\mathbf{D}_{np}F_s\mathbf{I})] \rhd_\Omega + E_{i,yj,y}\mathbf{I}_{\Omega y}^T \lhd F_\tau\mathbf{C}_{nn}F_s \rhd_\Omega \mathbf{I}_{\Omega y}\end{aligned} \tag{14}$$

where

$$\mathbf{I}_{\Omega y} = \begin{bmatrix} 0 & 0 & 1 \\ 1 & 0 & 0 \\ 0 & 1 & 0 \end{bmatrix} \quad \lhd \ldots \rhd_\Omega = \int_\Omega \ldots\,\mathrm{d}\Omega \tag{15}$$

$$(E_{ij},E_{ij,y},E_{i,yj},E_{i,yj,y}) = \int_l (N_iN_j,N_iN_{j,y},N_{i,y}N_j,N_{i,y}N_{j,y})\,\mathrm{d}y \tag{16}$$

The symbol $\lhd \ldots \rhd_\Omega$ indicates integration over the cross-section. The virtual variation of the work of inertial loadings is

$$\delta L_{\text{ine}} = \int_V \delta\mathbf{u}^T\rho\ddot{\mathbf{u}}\,\mathrm{d}V \tag{17}$$

where ρ is the density of the material and $\ddot{\mathbf{u}}$ is the acceleration vector. By retrieving Eq. (9), δL_{ine} can be rewritten in terms of virtual nodal displacements as follows:

$$\delta L_{\text{ine}} = \delta\mathbf{q}_{\tau i}^T \int_\Omega \rho(F_\tau\mathbf{I})\left[\int_l N_iN_j\mathrm{d}y\right](F_s\mathbf{I})\,\mathrm{d}\Omega\ \ddot{\mathbf{q}}_{sj} \tag{18}$$

where $\ddot{\mathbf{q}}$ is the nodal acceleration vector. The virtual variation of the work of inertial loadings can be finally expressed in the following compact notation:

$$\delta L_{\text{ine}} = \delta \mathbf{q}_{\tau i}^T \, [\rho E_{ij} \lhd F_\tau F_s \rhd_\Omega \mathbf{I}] \ddot{\mathbf{q}}_{sj} = \delta \mathbf{q}_{\tau i}^T \mathbf{M}^{ij\tau s} \ddot{\mathbf{q}}_{sj} \tag{19}$$

The 3×3 *fundamental nucleus* of the mass matrix presented in Eq. (19) is therefore a diagonal matrix. The virtual work of external loadings variationally consistent with the above method is here derived for the case of a generic concentrated load $\mathbf{P} = \{P_{u_x} \; P_{u_y} \; P_{u_z}\}^T$ acting on the load application point (x_P, y_P, z_P). By using Eq. (9), δL_{ext} becomes

$$\delta L_{\text{ext}} = \delta \mathbf{u}^T \mathbf{P} = \delta \mathbf{q}_{\tau i}^T F_\tau N_i \mathbf{P} = \delta \mathbf{q}_{\tau i}^T \mathbf{F}_{\tau i} \tag{20}$$

where F_τ is evaluated in (x_P, z_P) and N_i is calculated in y_P. Any other loading condition can be similarly treated. From Eqs. (11), (13), (19), and (20) the governing equation of motion can be derived through a finite element assembly procedure:

$$\mathbf{M}\ddot{\mathbf{q}} + \mathbf{K}\mathbf{q} = \mathbf{F} \tag{21}$$

where $\mathbf{M}$ is the mass matrix, $\mathbf{K}$ is the stiffness matrix and $\mathbf{F}$ is the vector of equivalent nodal forces. It should be noted that no assumptions on the expansion order have been made so far. Therefore, it is possible to obtain variable kinematic 1D models without changing the formal expression of the nucleus components. Thanks to the CUF, the present model is invariant with respect to the order of the beam theory and the type of element used in the finite element axial discretization. Shear locking is corrected through selective integration [1]. The Newmark time integration scheme [1], widely used in structural dynamics, is here employed. The equation of motion at time $t+\Delta t$ is then

$$\mathbf{M}\ddot{\mathbf{q}}_{t+\Delta t} + \mathbf{K}\mathbf{q}_{t+\Delta t} = \mathbf{F}_{t+\Delta t} \tag{22}$$

The step-by-step solution of Eq. (22) is computed by introducing the Newmark approximations for the displacements and velocities within the time step Δt:

$$\begin{aligned} \dot{\mathbf{q}}_{t+\Delta t} &= \dot{\mathbf{q}}_t + [(1-\delta)\ddot{\mathbf{q}}_t + \delta \ddot{\mathbf{q}}_{t+\Delta t}]\Delta t \\ \mathbf{q}_{t+\Delta t} &= \mathbf{q}_t + \dot{\mathbf{q}}_t \Delta t + [(1/2-\alpha)\ddot{\mathbf{q}}_t + \alpha \ddot{\mathbf{q}}_{t+\Delta t}]\Delta t^2 \end{aligned} \tag{23}$$

The values $\delta = 0.5$ and $\alpha = 0.25$ are employed for the related constants [1]. In general, any kind of dynamic loadings such as concentrated, distributed, and traveling loads with arbitrary time-dependence can be taken into account by the present formulation. Although the damping is not considered in the present paper, the formulation easily permits the introduction of a damping matrix $\mathbf{C}$, for example a Rayleigh damping $\mathbf{C} = \gamma\mathbf{M} + \beta\mathbf{K}$, in Eqs. (21) and (22).

5. Numerical results and discussion

As mentioned above, the present work concerns the first implementation of one-dimensional CUF models in the dynamic response analysis of slender structures. A preliminary assessment to test the accuracy of finite elements based on the CUF in a Newmark direct integration process is therefore required. Some reference cases retrieved from the structural dynamics literature [47] are taken as benchmark examples. Moreover, a number of thin-walled structures under dynamic loads are afterwards analyzed through refined 1D theories in order to highlight the shell-type capabilities of the formulation.

5.1. Compact square section

A square simply supported cross shaped beam is considered, see Fig. 1. The sides of the cross-section are equal to 0.1 m, whereas the span-to-height ratio L/h is equal to 100. This slender structure is modeled through a one-dimensional mesh of 10 B4 finite elements along the y-axis, as done for all the following analyses. In this paper, the isotropic material considered is aluminium: Young's modulus $E = 69$ GPa, Poisson's ratio $\nu = 0.33$, and density $\rho = 2700$ kg m^{-3}.

The first assessment case is a single harmonic force applied at the mid-span section of the beam:

$$P_z(t) = P_{z0} \sin(\omega t), \; y_L = L/2 \tag{24}$$

where $P_{z0} = 1000$ N is the amplitude of the sinusoidal load with angular frequency $\omega = 7$ rad s^{-1}. The analytical undamped dynamic response of an Euler–Bernoulli beam made of isotropic material and loaded by this kind of force is well-known [47]. Let ω_1 be the fundamental angular frequency of the beam corresponding to a bending modal shape. For the sake of

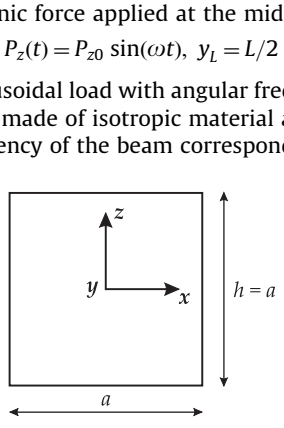

Fig. 1. Compact square cross-section.

brevity, when $\omega < \omega_1$ some reference values for the maximum transverse dynamic and static deflections occurring at the load application point are reported here:

$$u_{z\,\max,\mathrm{DYN}}^{\mathrm{anal}} \cong \frac{2P_{z0}L^3}{\pi^4 EI}\frac{1}{1-\omega/\omega_1}, \quad u_{z\,\max,\mathrm{ST}}^{\mathrm{anal}} = \frac{P_{z0}L^3}{48EI} \cong \frac{2P_{z0}L^3}{\pi^4 EI} \tag{25}$$

$$\frac{u_{z\,\max,\mathrm{DYN}}^{\mathrm{anal}}}{u_{z\,\max,\mathrm{ST}}^{\mathrm{anal}}} \cong \frac{1}{1-\omega/\omega_1} \tag{26}$$

where I is the moment of inertia of the beam cross-section.

The numerical dynamic response of the system is investigated through direct time integration via the Newmark method over the interval [0,8] s. Since the analytical solution refers to an Euler–Bernoulli beam, for a proper comparison the analysis involves that classical beam theory, which is obtained as a particular case of the first-order CUF model. Here, the Newmark method is unconditionally stable. However, the numerical solution approaches the reference trend as the time step Δt decreases. A convergence study is carried out to evaluate the dependence of the results on the time step chosen. The time-history of the transverse displacement u_z at the mid-span section is depicted in Fig. 2. It is noteworthy that the choice of $\Delta t = 0.08$ s represents a coarse time discretization for this problem, whereas a good agreement with the analytical deflection is achieved for $\Delta t = 0.004$ s. The dynamic response is approximately the sum of two sinusoidal functions with angular frequencies equal to ω and ω_1. The maximum dynamic displacement computed through FEs based on EBBM differs in about 0.03 percent from the analytical value, as reported in Table 1. It occurs for $t = 3.816$ s at the mid-span beam section. The static solution of the system is also evaluated by disabling the inertial contribution of the mass matrix. As expected, it is a time-dependent sinusoid with the same frequency as that of the point force. Unlike the dynamic case, the amplitude is constant and equal to $u_{z\,\max,\mathrm{ST}}^{\mathrm{anal}}$.

The time-response analysis is also conducted through refined beam models. Table 1 summarizes the maximum dynamic and static displacements for the third- and seventh-order models. However, for this case the increase of the theory expansion order N does not reveal any remarkable difference in comparison with Euler–Bernoulli beam theory. In fact, the use of a compact square section for a slender beam subjected to a bending load restricts the local effects of the beam cross-section, which are eventually detectable by the higher order terms of the beam displacement field. In confirmation of this fact, the value of the fundamental bending frequency of the beam ω_1 is substantially the same for all the theories involved, as evident from Table 1. EBBM is therefore an effective theory for this case.

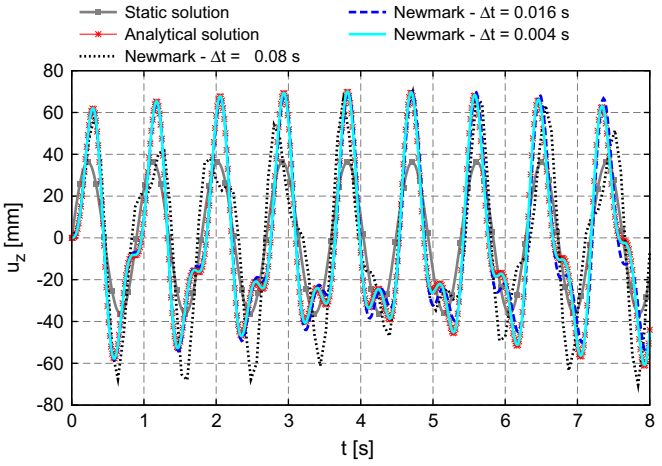

Fig. 2. Effect of the time step Δt on the transverse displacement at the mid-span section. Square cross-section case. Sinusoidal load. EBBM.

Table 1
Maximum dynamic and static displacements for different beam models. Square cross-section case. Sinusoidal load. $\Delta t = 0.004$ s for the Newmark method.

Theory	$u_{z\,\max,\mathrm{DYN}}$	$u_{z\,\max,\mathrm{ST}}$	ω_1	$\frac{u_{z\,\max,\mathrm{DYN}}}{u_{z\,\max,\mathrm{ST}}}$	$\frac{1}{1-\omega/\omega_1}$
Analytical	70.0116	36.2319	14.4030	1.9323	1.9456
EBBM	69.9886	36.2318	14.4024	1.9317	1.9456
$N=3$	70.0232	36.2427	14.4006	1.9321	1.9459
$N=7$	70.0233	36.2428	14.4006	1.9321	1.9459

The second assessment consists in a single sinusoidal force starting from the left support and traveling along the beam axis with a constant velocity v_y:

$$P_z(t) = P_{z0}\sin(\omega t), \quad y_L(t) = v_y t \tag{27}$$

The velocity v_y is set to 1.25 m s^{-1} so that the force covers the beam length L in the interval [0, 8] s. The analytical dynamic response to this load can be found in [47]. Unlike the nontraveling load case, in this second assessment the maximum displacement of the beam is not placed at the mid-span section for both the static and dynamic analyses. Nevertheless, as in the previous case, the time-dependent displacement of the mid-span section is investigated through EBBM and plotted in Fig. 3. The influence of the time step exploited in the Newmark method is less evident with respect to the nontraveling load case. However, the choice of $\Delta t = 0.004$ s is again an appropriate time discretization. In fact, the amplitude of the curve obtained with $\Delta t = 0.08$ s noticeably differs from the analytical benchmark even over $t = 2$ s and this error is likely to propagate dramatically in even longer simulations. The inertial effect due to the mass matrix emphasizes the transverse deflection of the beam with respect to the static response. For the sake of brevity, the results for refined theories are not reported here because there is no noticeable difference with Euler–Bernoulli beam theory.

A static force P_{z0} advancing along the beam axis with the same velocity is considered as a third assessment case:

$$P_z(t) = P_{z0}, \quad y_L(t) = v_y t \tag{28}$$

At first, the inertial effect is neglected in order to evaluate the static behavior of the beam, in terms of the displacement $u_z(y = L/2, t)$ of the mid-span section. This time-dependent displacement is described by the continuous cubic function illustrated by the square symbols in Fig. 4. The static curve is defined on two subsets and is symmetrical with respect to

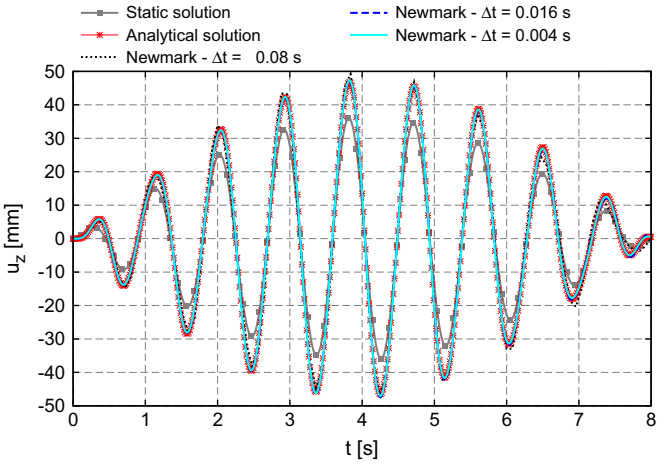

Fig. 3. Effect of the time step Δt on the transverse displacement at the mid-span section. Square cross-section case. Sinusoidal traveling load. EBBM.

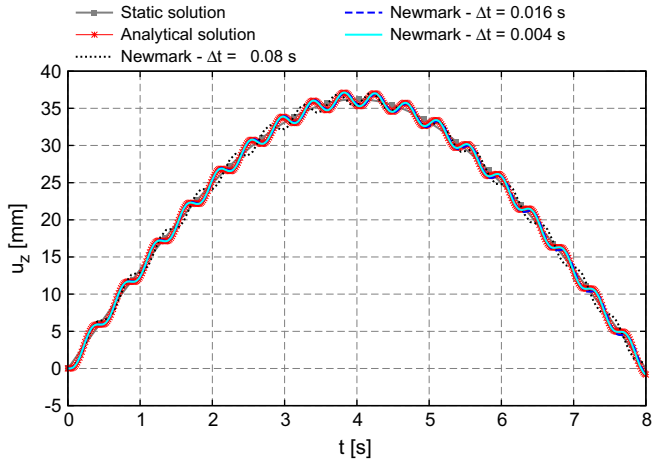

Fig. 4. Effect of the time step Δt on the transverse displacement at the mid-span section. Square cross-section case. Constant traveling load. EBBM.

$t=4$ s. In fact, for Euler–Bernoulli beam theory:

$$u_z(y=L/2,t)=\begin{cases}\dfrac{P_{z0}}{48EI}(3L^2-4(v_yt)^2)(v_yt), & 0\le v_yt\le L/2\\ \dfrac{P_{z0}}{48EI}(-L^2+8L(v_yt)-4(v_yt)^2)(L-(v_yt)), & L/2\le v_yt\le L\end{cases} \tag{29}$$

For the static analysis, it is possible to demonstrate that the maximum deflection of the beam, $u_{z\,\max}=P_{z0}L^3/48\,EI$, is placed at $y=L/2$ for $t_{u_{z\,\max}}=4$ s, that is for $y_L=v_yt=5$ m. On the contrary, the dynamic response curve oscillates over the static cubic function and is no longer symmetrical. As a result, the maximum value of u_z during the considered time interval is no longer reached at the mid-span section. The Newmark method fails to compute the frequency of this oscillating trend through a coarse time discretization ($\Delta t=0.08$ s). Instead, the direct time integration with $\Delta t=0.004$ s ensures a convergent solution by approaching the analytical results across the entire time interval of study. Furthermore, the error in computing the maximum dynamic displacement at $y=L/2$ decreases as Δt decreases. As shown in Table 2, the same occurs for the corresponding time instant $t_{u_{z\,\max}}$. In fact, the position of the load application point $y_L(t_{u_{z\,\max}})$ at the time instant $t_{u_{z\,\max}}$ is moderately different from the analytical value, except for the refined value $\Delta t=0.004$ s.

5.2. Thin-walled rectangular section

The assessment procedure on compact beams is completed. A clamped-free beam with a thin-walled rectangular cross-section is now introduced. As illustrated in Fig. 5, the width a of the section is equal to 1 m and the width-to-height ratio is equal to 10. The thickness t of the skin is constant and equal to 0.005 m. The beam is relatively short since the span-to-width ratio L/a is now equal to 10. The section at $y=2.5$ m is loaded by a concentrated force P_z. On this section, six points are chosen as characteristic positions. The application point is denoted as point 1 in Fig. 5. The effect of the point load on this thin-walled section is evaluated through a preliminary static analysis with $P_z=10\,000$ N. This case cannot be consistent with the kinematic hypotheses which classical beam models are based on. Classical models are therefore not expected to yield accurate results. In fact, while EBBM assumes an undeformed section, the increase of the expansion order N provides a remarkable shell-like deformation of the loaded cross-section. Fig. 6 illustrates that the upper skin is particularly deflected due to the position of P_z at point 1. However, at least a 10th-order model (6138 DOFs) is necessary to detect such an effect and simulate the FE NASTRAN solution well, obtained through a 396 000 DOFs analysis.

A time-dependent sinusoidal load with amplitude $P_{z0}=-10\,000$ N and angular frequency $\omega=30$ rad s^{-1} is applied at point 1. Given the static results, a 10th-order structural model is considered in the dynamic analysis over the interval [0,1.5] s. Fig. 7 plots the convergence of the solution as the time step used in the Newmark method decreases. For instance, point 3 is taken as a control point. Again, Δt affects the correct evaluation of the amplitude and frequency of the beam

Table 2
Maximum displacement of the mid-span square section and corresponding time instant for different time steps through the Newmark method. Constant traveling load. EBBM.

Analysis	$u_{z\,\max}$	$t_{u_{z\,\max}}$	$y_L(t_{u_{z\,\max}})/L$
Newmark $\Delta t=0.08$ s	36.9617	4.160	0.52
Newmark $\Delta t=0.016$ s	37.1458	3.840	0.48
Newmark $\Delta t=0.004$ s	37.1292	3.824	0.47
Analytical solution	37.1185	3.824	0.47
Static solution	36.2319	4.000	0.50

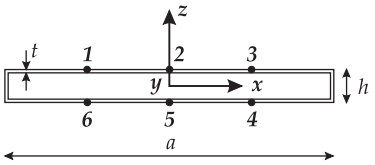

Fig. 5. Thin-walled rectangular cross-section.

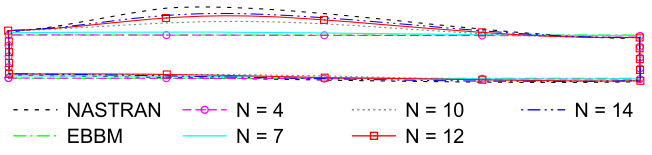

Fig. 6. Static deformation of the loaded thin-walled rectangular cross-section.

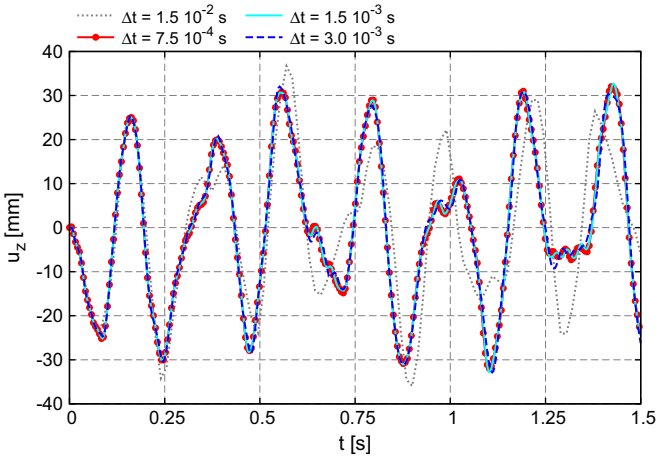

Fig. 7. Effect of the time step Δt on the transverse displacement of point 3. Thin-walled rectangular cross-section case, $N=10$.

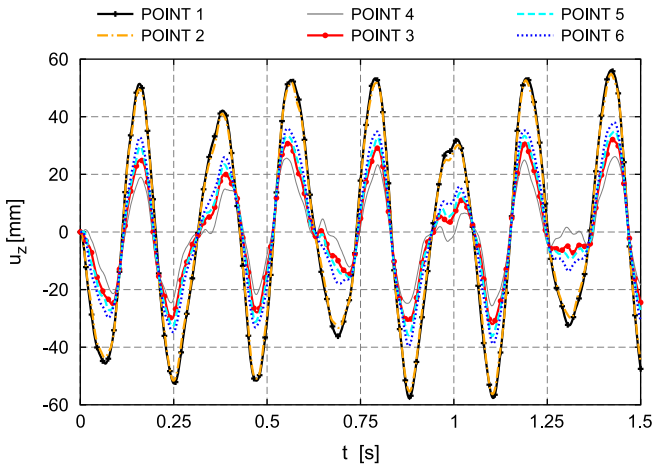

Fig. 8. Dynamic response of different points on the loaded cross-section. Thin-walled rectangular cross-section case, $\Delta t = 7.5 \times 10^{-4}$ s, $N=10$.

dynamic response. It can be demonstrated that this convergence is also required for classical and lower order theories. Once an appropriate Δt is chosen, the transverse displacement is evaluated for points 1–6 and depicted in Fig. 8. As expected, u_z reaches the maximum value at loading point 1, whose trend is described mainly by an oscillation with angular frequency equal to ω. The other points seem to be affected in a different way by some local oscillations due to inertial effects, see in particular point 4. Such effects can be observed thanks to higher order terms. In fact, for EBBM the six curves would coincide perfectly, given the undeformed section hypothesis of classical models.

Fig. 9 displays the response of point 1 computed for different theories. EBBM and the fourth-order model provide very similar results. For $N=7$ the maximum displacement increases, but it is via the 10th-order model that u_z dramatically rises, even over 250 percent with respect to EBBM and $N=4$. The difference consists not only in the amplitude of the oscillation, but also in the trend shape. Unlike lower order models, for $N=10$ the displacement of point 1 vs. time is an oscillating curve dominated by the angular frequency of the load. The same behavior does not occur at point 4, which lies on the lower skin of the section. The refinement of models does not reveal a striking difference in maximum displacement whereas their trend shapes are considerably dissimilar, see Fig. 10. Since higher order terms are powerful in evaluating the section deformation, refined models are able to detect local shell-like oscillations related to different inertial accelerations of points over the loaded section. Table 3 summarizes the results in terms of maximum displacement of points 1–6 obtained over the interval. Especially for $N=10$ these values are very different within the section and correspond to different time instants.

5.3. *Thin-walled circular section*

A thin-walled circular cross-section is considered in the last analysis cases of the present work. Thus the beam to be analyzed is now a complete circular cylindrical shell. Before investigating the dynamic response, the present one-dimensional

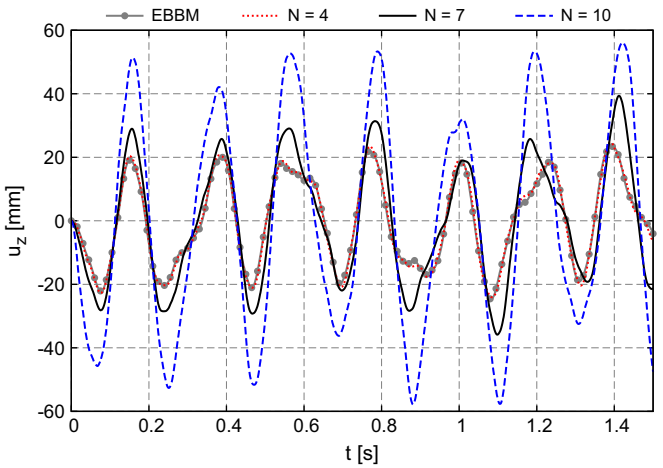

Fig. 9. Time-dependent transverse displacement of point 1 for different theories. Thin-walled rectangular cross-section case, $\Delta t = 7.5 \times 10^{-4}$ s.

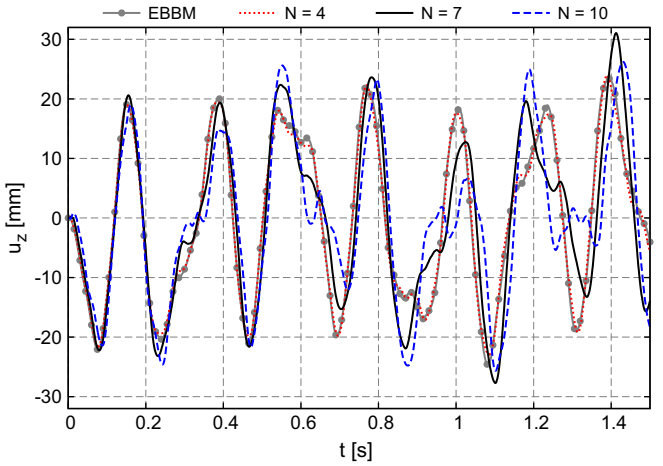

Fig. 10. Time-dependent transverse displacement of point 4 for different theories. Thin-walled rectangular cross-section case, $\Delta t = 7.5 \times 10^{-4}$ s.

Table 3
Maximum displacement (mm) of points 1–6 and corresponding time instant for different theories. Thin-walled rectangular cross-section case, $\Delta t = 7.5 \times 10^{-4}$ s.

$u_{z\,\max}$	EBBM	N=4	N=7	N=10
Point 1	−24.660	24.812	39.359	−57.838
	(1.08225 s)	(1.38975 s)	(1.41225 s)	(0.88125 s)
Point 2	−24.660	24.363	37.007	−56.280
	(1.08225 s)	(1.38975 s)	(1.41225 s)	(1.10325 s)
Point 3	−24.660	23.964	32.944	32.071
	(1.08225 s)	(1.38900 s)	(1.41300 s)	(1.42425 s)
Point 4	−24.660	23.964	31.055	26.193
	(1.08225 s)	(1.38900 s)	(1.41225 s)	(1.43100 s)
Point 5	−24.660	24.362	34.357	−36.156
	(1.08225 s)	(1.38975 s)	(1.41225 s)	(1.10250 s)
Point 6	−24.660	24.810	37.419	−39.633
	(1.08225 s)	(1.38975 s)	(1.41225 s)	(0.87900 s)

structural model should be directly assessed by comparison with free vibration results based on exact analysis of Ref. [48] and three-dimensional analysis in [49]. Armenàkas et al. [48] provided exact natural frequencies of harmonic elastic waves propagating in an infinitely long isotropic hollow cylinder. However, this work may be used directly in obtaining the frequency of standing waves propagating in simply supported shells of finite length. The analyses in [48] were based on closed form solutions of the governing three-dimensional equations which were obtained in terms of Bessel functions. In [49] governing

Table 4
Comparison of frequency parameters $\overline{\omega}$ based on the present 1D CUF and 3D analysis for a circular cylindrical shell ($m=1$).

n		$N=4$	$N=7$	$N=9$	Exact 3D [48]	3D [49]
2	I	1.0804	1.0620	1.0620	1.0623	1.0624
	II	2.3758	2.3745	2.3744	2.3744	2.3745
4	I	0.9937	0.8838	0.8819	0.8823	0.8826
	II	2.9118	2.7160	2.7159	2.7159	2.7159
6	I	1.7500	0.8388	0.8112	0.8093	0.8096
	II	4.1441	3.1562	3.1534	3.1533	3.1533

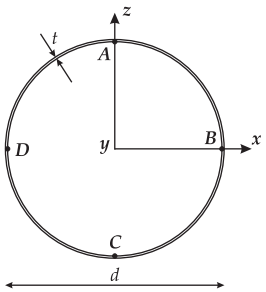

Fig. 11. Thin-walled circular cross-section.

equations of three-dimensional linear elasticity were instead solved by using an iterative approach based on the introduction of fictitious layers along the shell thickness.

A comparison is presented in Table 4 for a simply supported shell with outer diameter d equal to 1.05 m, thickness t equal to 0.05 m, and length L equal to 0.5 m, see Fig. 11. This structure represents a very severe test case for the present one-dimensional model, since it is a very short cylinder ($L/d<0.5$) with a thin-walled cross-section. Classical beam theories are completely ineffective in studying this kind of structures. Different values of the circumferential half-wave number n ($2n$ in [48]) are investigated, whereas the axial half-wave number m is set to 1. In Table 4 the two first frequency parameters $\overline{\omega}$ based on the present 1D CUF model are compared with corresponding 3D results obtained in Refs. [48,49] according to the following equation:

$$\overline{\omega}=\frac{\Omega\pi L}{t\sqrt{2}}=\omega L\sqrt{\frac{\rho(1+\nu)}{E}} \tag{30}$$

where Ω is the frequency parameter used in [48] and ω is the natural angular frequency of vibration. Table 4 shows that it is necessary to enhance the displacement field with higher order terms to correctly describe the dynamic behavior of the cylinder. This statement is true especially for vibrating modes with a high half-wave number. For instance, a fourth-order model provides good results for $n=2$, whereas the frequency parameters computed for $n=6$ are clearly wrong. The results of the present 1D CUF model (with $N=9$) are in excellent agreement with the results based on three-dimensional elasticity solutions [48,49]. An accuracy in three significant figures is achieved, and this validates the correctness of the present analysis.

A clamped–clamped beam with a thin-walled circular cross-section is considered in the last analysis case of the present work. The outer diameter of the cylinder d is equal to 0.1 m whereas the thickness is 0.001 m. The span-to-diameter ratio L/d is equal to 10. As displayed in Fig. 11, four particular points are considered over the mid-span cross-section. Four concentrated forces are applied at points A, B, C and D within the thin-walled cross-section, in an outward direction. They are time-dependent sinusoids with amplitude $P_{z0}=10\,000$ N and a phase shift:

$$\begin{aligned} P_{zA}(t)&=P_{z0}\sin(\omega t+\phi_A), \quad \phi_A=0^\circ\\ P_{xB}(t)&=P_{z0}\sin(\omega t+\phi_B), \quad \phi_B=30^\circ\\ P_{zC}(t)&=-P_{z0}\sin(\omega t+\phi_C), \quad \phi_C=60^\circ\\ P_{xD}(t)&=-P_{z0}\sin(\omega t+\phi_D), \quad \phi_D=90^\circ \end{aligned} \tag{31}$$

where the angular frequency is $\omega=100$ rad s^{-1}. The dynamic response of the structure is evaluated over the time interval [0,0.025] s by involving classical as well as refined 1D models. The deformed configuration of the mid-span section at $t=0$ s is presented in Fig. 12 and compared with NASTRAN shell-FE solution. EBBM and TBM detect only a rigid translation of the cross-section. The fourth-order theory shows a global deformation but cannot detect any local effect due to the concentrated loads. With $N=7$ the refined elements are able to detect the shell-like displacement field of all the cross-section points except the loading ones. An expansion order N at least equal to 10 is necessary to obtain a detailed description of the loading points displacement field. This conclusion is consistent with the results obtained through CUF models by Carrera et al. [50].

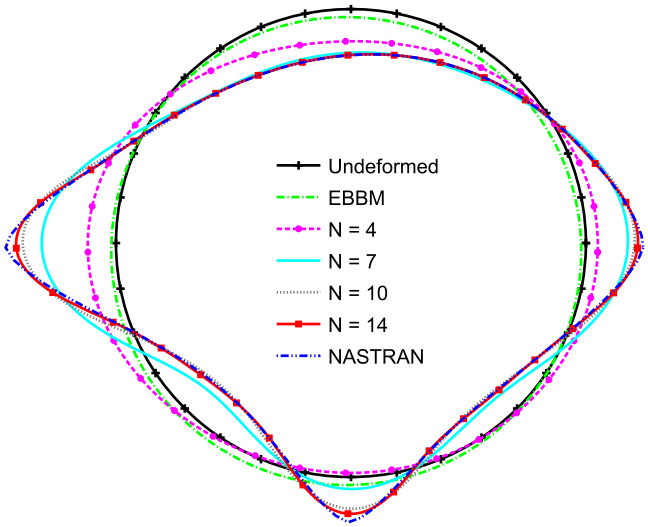

Fig. 12. Static response of the mid-span circular cross-section, $t=0$ s.

Table 5
Displacements (mm) of the loading points A and D for different FE models. Thin-walled cylinder case, $t=0$ s.

Theory	u_{xD}	Error u_{xD}	u_{zA}	Error u_{zA}	DOFs
EBBM	−0.9906	−95.78%	−1.7157	−82.64%	93
TBM	−1.1453	−95.12%	−1.9838	−79.93%	155
$N=1$	−2.0937	−91.08%	−1.4362	−85.47%	271
$N=3$	−2.9313	−87.51%	−3.5311	−64.27%	930
$N=4$	−5.9690	−74.56%	−6.8900	−30.29%	1395
$N=7$	−15.7213	−32.99%	−9.3591	−5.31%	3348
$N=10$	−19.7523	−15.81%	−9.7314	−1.54%	6138
$N=14$	−21.1939	−9.67%	−9.8418	−0.43%	11 160
NASTRAN	−23.4628	–	−9.8840	–	250 000

Table 5 summarizes the transverse displacements of loading points A and D at $t=0$ s. The third and fifth columns present the percentage error computed with respect to the NASTRAN solution, taken as a reference, for u_{xD} and u_{zA}, respectively. As expected, the computation of local displacements on these loading points is not trivial for lower order models and impossible for classical models. A slight improvement is noticed for $N=7$, but the error decreases remarkably for an expansion order higher than 10. The last column shows the total number of degrees of freedom, DOFs, for each model. A good convergent trend is observed as N increases with a considerably smaller computational effort than that required by the reference shell model. In Fig. 13 the static three-dimensional deformation of the cylinder computed via $N=10$ is graphically compared with NASTRAN shell solution. The spectrum used on the surface corresponds to the resultant displacement. As expected, the mid-span section is subjected to the overall maximum deflection due to the concentrated loads. Fig. 13 emphasizes the capabilities of the proposed refined model in describing typical shell-like lobes over the thin-walled structure with a sizeable reduction in computational cost in terms of DOFs (6138 vs. 250 000).

As far as the dynamic response is concerned, the analysis involves variable kinematic models with an expansion order N up to 10 because of the considerations exposed above for the static case. The mid-span cross-section remains the most stressed section and the high sensitivity of its shape to the point loads is detectable for higher order models. For instance, the configuration at the final time instant $t=0.025$ s is depicted in Fig. 14. According to Fig. 12, $N=4$ is again unable to detect any local effect near the loading points; it only detects a global deflection of the circular section. On the contrary, with $N=7$ and $N=10$ the proposed 1D model makes it possible to take into account local deformations typical of a shell-like behavior.

6. Conclusions

This paper presents the extension of refined one-dimensional models to the dynamic response analysis of isotropic thin-walled structures. Variable kinematic 1D finite elements were formulated on the basis of Carrera Unified Formulation, CUF, by exploiting a systematic procedure that leads to governing FE matrices whose form does not depend on the order of expansion used for the displacement unknowns over the cross-section.

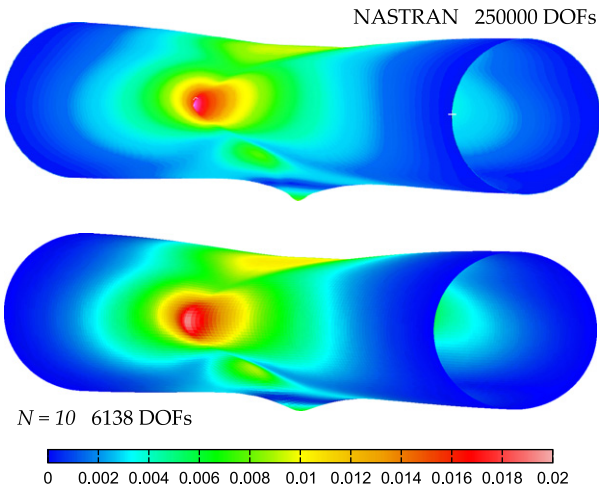

Fig. 13. Static three-dimensional resultant displacement of the thin-walled cylinder, $t=0$ s.

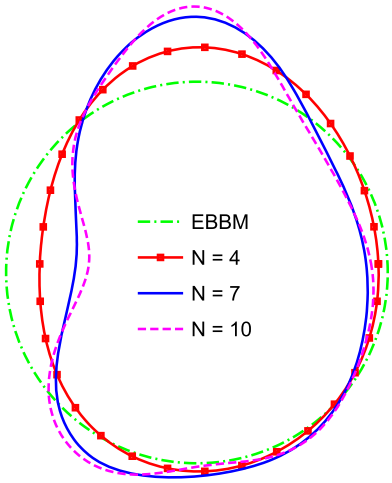

Fig. 14. Deformation of the mid-span circular cross-section for different beam models, $t=0.025$ s.

Several analyses were carried out to assess and enhance the advantages of higher order 1D CUF models in evaluating the dynamic response of slender structures. In particular, a cylinder with a thin-walled circular cross-section subjected to harmonic out of phase loadings was studied. Comparing results with three-dimensional elasticity solutions and shell-type solutions obtained by commercial FE software, the following main conclusions can be drawn:

1. the effectiveness of higher order terms over the cross-section deformation is enhanced when thin-walled geometries are adopted;
2. since classical beam theories assume an undeformed section, they become ineffective in the case of thin-walled geometries;
3. in-plane deformations due to time-dependent internal loadings are accurately detected by the proposed 1D models.

As far as numerical implementation is concerned:

a. the proposed models did not introduce additional numerical problems in direct time integration with respect to classical beam theories;
b. the convergence of the Newmark method was achieved for both the classical and higher order FE models.

According to previous works involving 1D CUF models, the paper confirms that the increase of the expansion order is not only important for static and free vibration analyses; it is also crucial for the dynamic response of beam-like structures.

The implementation of 1D CUF models in the Newmark time integration scheme has revealed the shell-type capabilities of such refined models in accurately describing the dynamic behavior of thin-walled structures with a sizeable reduction in computational cost.

References

[1] K. Bathe, *Finite Element Procedures*, Prentice Hall, Upper Saddle River, New Jersey, 1996.
[2] L. Euler, De curvis elasticis, Bousquet, Lausanne and Geneva, 1744.
[3] S. Timoshenko, On the correction for shear of the differential equation for transverse vibrations of prismatic bars, *Philosophical Magazine* 41 (1921) 744–746.
[4] E. Carrera, G. Giunta, Refined beam theories based on a unified formulation, *International Journal of Applied Mechanics* 2 (2010) 117–143.
[5] E. Carrera, G. Giunta, M. Petrolo, *Beam Structures: Classical and Advanced Theories*, John Wiley & Sons, 2011.
[6] W. Yu, V. Volovoi, D. Hodges, X. Hong, Validation of the variational asymptotic beam sectional analysis (VABS), *AIAA Journal* 40 (2002) 2105–2113.
[7] N. Silvestre, D. Camotim, Second-order generalised beam theory for arbitrary orthotropic materials, *Thin-Walled Structures* 40 (2002) 791–820.
[8] Y.C. Fung, *Biomechanics: Mechanical Properties of Living Tissues*, 2nd ed. Springer, New York, 1993.
[9] J.D. Anderson, *Fundamentals of Aerodynamics*, 5th ed. McGraw-Hill, 2010.
[10] L. Librescu, S. Na, Dynamic response of cantilevered thin-walled beams to blast and sonic-boom loadings, *Shock and Vibration* 5 (1998) 23–33.
[11] F.T.K. Au, Y.S. Cheng, Y.K. Cheung, Vibration analysis of bridges under moving vehicles and trains: an overview, *Progress in Structural Engineering and Materials* 3 (2001) 299–304.
[12] X. Qiu, V.S. Deshpande, N.A. Fleck, Finite element analysis of the dynamic response of clamped sandwich beams subject to shock loading, *European Journal of Mechanics A/Solids* 22 (2003) 801–814.
[13] M.R. Lindeburg, K.M. McMullin, *Seismic Design of Building Structures*, 9th ed. Professional Publications, 2008.
[14] S.R. Marur, T. Kant, On the performance of higher order theories for transient dynamic analysis of sandwich and composite beams, *Computers & Structures* 65 (1997) 741–759.
[15] K. Kapania, S. Raciti, Recent advances in analysis of laminated beams and plates, part II: vibrations and wave propagation, *AIAA Journal* 27 (1989) 935–946.
[16] N.G. Stephen, M. Levinson, A second order beam theory, *Journal of Sound and Vibration* 67 (1979) 293–305.
[17] P.R. Heyliger, J.N. Reddy, A higher order beam finite element for bending and vibration problems, *Journal of Sound and Vibration* 126 (1988) 309–326.
[18] K.P. Soldatos, I. Elishakoff, A transverse shear and normal deformable orthotropic beam theory, *Journal of Sound and Vibration* 155 (1992) 528–533.
[19] M. Levinson, A new rectangular beam theory, *Journal of Sound and Vibration* 74 (1981) 81–87.
[20] Z. Rychter, On the accuracy of a beam theory, *Mechanics Research Communications* 14 (1987) 99–105.
[21] W.B. Bickford, A consistent higher-order beam theory, *Developments in Theoretical and Applied Mechanics* 11 (1982) 137–150.
[22] T. Kant, A. Gupta, A finite element model for a higher-order shear deformable beam theory, *Journal of Sound and Vibration* 125 (1988) 193–202.
[23] S.R. Marur, T. Kant, Free vibration analysis of fiber reinforced composite beams using higher order theories and finite element modelling, *Journal of Sound and Vibration* 194 (1996) 337–351.
[24] S.R. Marur, T. Kant, On the angle ply higher order beam vibrations, *Computational Mechanics* 40 (2007) 25–33.
[25] T. Kant, S.R. Marur, G.S. Rao, Analytical solution to the dynamic analysis of laminated beams using higher order refined theory, *Composite Structures* 40 (1997) 1–9.
[26] P. Subramanian, Dynamic analysis of laminated composite beams using higher order theories and finite elements, *Composite Structures* 73 (2006) 342–353.
[27] R. Ganesan, A. Zabihollah, Vibration analysis of tapered composite beams using a higher-order finite element, part I: formulation, *Composite Structures* 77 (2007) 306–318.
[28] R. Ganesan, A. Zabihollah, Vibration analysis of tapered composite beams using a higher-order finite element, part II: parametric study, *Composite Structures* 77 (2007) 319–330.
[29] M. Şimşek, T. Kocatürk, Free vibration analysis of beams by using a third-order shear deformation theory, *Sādhanā* 32 (2007) 167–179.
[30] X. Tong, B. Tabarrok, K.Y. Yeh, Vibration analysis of Timoshenko beams with non-homogeneity and varying cross-section, *Journal of Sound and Vibration* 186 (1995) 821–835.
[31] S. Ramalingerswara Rao, N. Ganesan, Dynamic response of tapered composite beams using higher order shear deformation theory, *Journal of Sound and Vibration* 187 (1995) 737–756.
[32] M.H. Kadivar, S.R. Mohebpour, Finite element dynamic analysis of unsymmetric composite laminated beams with shear effect and rotary inertia under the action of moving loads, *Finite Elements in Analysis and Design* 29 (1998) 259–273.
[33] L. Librescu, S. Na, Boundary control of free and forced oscillation of shearable thin-walled beam cantilevers, *European Journal of Mechanics – A/Solids* 17 (1998) 687–700.
[34] S. Na, L. Librescu, Dynamic response of elastically tailored adaptive cantilevers of nonuniform cross section exposed to blast pressure pulses, *International Journal of Impact Engineering* 25 (2001) 847–867.
[35] M.T. Piovan, V.H. Cortínez, Mechanics of thin-walled curved beams made of composite materials, allowing for shear deformability, *Thin-Walled Structures* 45 (2007) 759–789.
[36] M. Şimşek, Vibration analysis of a functionally graded beam under a moving mass by using different beam theories, *Composite Structures* 92 (2010) 904–917.
[37] E. Carrera, M. Petrolo, On the effectiveness of higher-order terms in refined beam theories, *Journal of Applied Mechanics* 78 (2011) 021013.1–021013.17.
[38] E. Carrera, M. Petrolo, Refined one-dimensional formulations for laminated structure analysis, *AIAA Journal* 50 (2012) 176–189.
[39] A. Varello, M. Petrolo, E. Carrera, A refined 1D FE model for the application to aeroelasticty of composite wings, *Proceedings of the IV International Conference on Computational Methods for Coupled Problems in Science and Engineering*, Kos Island, Greece, June 2011.
[40] E. Carrera, S. Brischetto, P. Nali, *Plates and Shells for Smart Structures: Classical and Advanced Theories for Modeling and Analysis*, John Wiley & Sons, 2011.
[41] E. Carrera, G. Giunta, P. Nali, M. Petrolo, Refined beam elements with arbitrary cross-section geometries, *Computers & Structures* 88 (2010) 283–293.
[42] E. Carrera, M. Petrolo, A. Varello, Advanced beam formulations for free vibration analysis of conventional and joined wings, *Journal of Aerospace Engineering* 25 (2012) 282–293.
[43] E. Carrera, M. Petrolo, P. Nali, Unified formulation applied to free vibrations finite element analysis of beams with arbitrary section, *Shock and Vibrations* 18 (2010) 485–502.
[44] R. Jones, *Mechanics of Composite Materials*, 2nd ed. Taylor and Francis, Philadelphia, 1999.
[45] E. Carrera, S. Brischetto, Analysis of thickness locking in classical, refined and mixed multilayered plate theories, *Composite Structures* 82 (2008) 549–562.

[46] E. Carrera, S. Brischetto, Analysis of thickness locking in classical refined and mixed theories for layered shells, *Composite Structures* 85 (2008) 83–90.
[47] E. Volterra, E.C. Zachmanoglou, *Dynamics of Vibrations*, C.E. Merrill Books, Columbus, 1965.
[48] A.E. Armenàkas, D.C. Gazis, G. Herrmann, *Free Vibrations of Circular Cylindrical Shells*, Pergamon Press, Oxford, 1969.
[49] K.P. Soldatos, V.P. Hadjigeorgiou, Three-dimensional solution of the free vibration problem of homogeneous isotropic cylindrical shells and panels, *Journal of Sound and Vibration* 137 (1990) 369–384.
[50] E. Carrera, M. Petrolo, A beam formulation with shell capabilities, *Proceedings of the* 51*st AIAA/ASME/ASCE/AHS/ASC Structures*, *Structural Dynamics*, *and Materials Conference*, Orlando, Florida, April 2010, AIAA Paper 2010–3021.